Combining Experimental and Computational Tools to Unravel Copper-Based Metallodrug Interactions With Proteins

Quim Peña, Iker Zapirain-Gysling, A. Jalila Simaan, Mercè Capdevila, Olga Iranzo, Òscar Palacios, Jean-Didier Maréchal, Pau Bayón

Wiley
Bioinorganic Chemistry and Applications
Volume 2025, Article ID 5551967, 16 pages
https://doi.org/10.1155/bca/5551967

WILEY

Research Article

Combining Experimental and Computational Tools to Unravel Copper-Based Metallodrug Interactions With Proteins

Quim Peña,[1,2,3] **Iker Zapirain-Gysling**,[1] **A. Jalila Simaan**,[2] **Mercè Capdevila**,[1] **Olga Iranzo**,[2] **Òscar Palacios**,[1] **Jean-Didier Maréchal**,[1] **and Pau Bayón**[1]

[1]*Chemistry Department, Faculty of Sciences, Universitat Autònoma de Barcelona, Cerdanyola Del Vallès, Barcelona 08193, Spain*
[2]*Aix Marseille University, CNRS, Centrale Marseille, iSm2, Marseille, France*
[3]*Institute for Experimental Molecular Imaging, RWTH Aachen University Hospital, Forckenbeckstrasse 55, Aachen 52074, Germany*

Correspondence should be addressed to Jean-Didier Maréchal; jeandidier.marechal@uab.cat and Pau Bayón; pau.bayon@uab.cat

Received 5 November 2024; Accepted 8 January 2025

Academic Editor: Enrico Rizzarelli

Metallodrugs are widely used in the treatment of several diseases, including cancer. Many bloodstream proteins exhibit high affinities for metals and metal-based compounds, and these interactions have been shown to impact metallodrug pharmacokinetics and pharmacodynamics, ultimately influencing their therapeutic performance. Several spectroscopic, spectrometric, and computational techniques have been used to further understand drug–protein binding modes at the molecular level over the last few years. However, there is still plenty of room to ascertain the full potential of integrated experimental–computational methodologies in the field of metallodrugs. These studies have mostly been limited to a few metal-containing systems, such as platinates and vanadium drugs. In this work, we aim to expand and validate the use of combined experimental–theoretical approaches in studying copper (Cu)-based drug interactions with proteins. To do so, a tetracoordinated Cu(II) complex has been employed as a practical case study, and its interactions with several relevant proteins using different experimental and computational techniques have been evaluated, including electron paramagnetic resonance spectroscopy, mass spectrometry, density functional theory, and protein–ligand docking calculations. Experimental data highlight interactions of the Cu(II) complex with albumin, myoglobin, and cytochrome C. Further insights into the preferential modes of binding were evaluated by density functional theory and docking calculations, which revealed three main outer surface binding sites for both albumin and myoglobin, as well as three preferential inner pockets in the case of albumin. The most relevant binding modes found for both proteins include noncoordinative interactions with the Cu(II) dimeric structure intact upon binding, as well as metal–ligand exchange and direct metal–amino acid coordination, mainly to glutamate/aspartate residues after cleavage of the dimer. Altogether, an example of the applicability of a mixed experimental–theoretical framework in the study of Cu-based drug interactions with relevant proteins is shown.

Keywords: albumin; cancer; copper; docking; metallodrug; protein binding

1. Introduction

Metal-based drugs are common in clinical treatments of diseases such as cancer, arthritis, anemia, and mental disorders [1, 2]. Compounds based on transition metals can adopt a wide variety of geometries that, allied with versatile electronic properties, types of metal–ligands, and oxidation states, offer a unique structural framework to design bioactive agents [1, 2]. These features have motivated the development of metal complexes based on platinum (Pt), gold (Au), copper (Cu), and iron (Fe), which exhibit a broad spectrum of therapeutic properties and mechanisms of action.

Many metallodrugs, including those for cancer therapy, are administered intravenously. As a result, their in vivo stability, speciation, and performance are strongly

influenced by their interactions with blood components [3]. The human serum proteome is composed of more than 10,000 proteins [3], of which a nonnegligible number is able to bind metals and metal-based compounds. In particular, highly abundant bloodstream proteins (e.g., human serum albumin [HSA], human serum transferrin [Tf], and hemoglobin), as well as others present in tissues and inside cells (e.g., myoglobin [Myo] and cytochrome C [Cyt]) [4], are prone to interact with metal-containing compounds [4, 5]. Such interactions depend on multiple factors, including the nature of the metal, its oxidation state, the metal–ligand, and the spatial rearrangement of atoms in the metal complex. In general, these imply the substitution of one or several metal–ligands of the first coordination sphere with different amino acid residues of the protein (i.e., direct metal coordination) and/or different (polar/hydrophobic) intermolecular interactions such as hydrogen bonding and van der Waals (vdW) forces [5–7].

The nature of these interactions plays a critical role in defining the pharmacological and toxicological profile of metallodrugs, and these can result in side effects and the development of resistance to treatments [8, 9]. Besides, protecting drugs from rapid metabolization or albumin binding has been shown to improve the biodistribution, target site accumulation, and therapeutic profile of drugs in some cases [2, 10–12]. Eventually, promoting interaction with bloodstream proteins such as HSA can also result in advantageous pharmacokinetic and pharmacodynamic features [10–12]. Therefore, it is clear that elucidating the modes of interaction of metallodrugs and metallodrug candidates with proteins is critical to understanding and potentially depicting their therapeutic profile. Yet, reaching such knowledge at the molecular level remains challenging with the currently available experimental methods. Well-resolved X-ray diffraction (XRD) structures of the metallodrug bound to its target are scarce, and most of the molecular and atomic interactions described for metallodrug–protein adducts are indirectly concluded from spectroscopic analysis. In recent years, efforts have been made to bring computational methods to predict the spatial layout of metallodrug–protein complexes with the emerging role of molecular docking and binding site predictors [13].

Molecular docking is a computational method to determine low-energy (stable) complexes between two molecular partners. One of its main goals in biochemistry and medicine is protein–ligand docking, which serves to predict the site and mode of binding of small molecules (ligand in docking terminology), such as drugs and drug candidates with a protein receptor [14]. Protein–ligand docking has become a standard and valuable element in the medicinal chemistry toolkit, particularly in drug discovery of small organic molecules [15]. When it comes to metallodrugs, though, like in many fields of molecular modeling, the presence of the metal increases the complexity of simulation and modeling. Thanks to different advances made in this field (including by our group), several studies based on metal-compatible dockings have been recently reported; many centered on Pt complexes and some on vanadium (V) systems [16]. However, there are comparatively few examples where experimental–theoretical methodologies have been combined in the study of the biological interactions of (therapeutic) Cu-based compounds [17, 18].

Taking the above concepts together, and given the high chemical, biological, and medicinal values of elucidating the interactions of metal-based compounds with biomolecules, we here aim to fundamentally expand on the applicability of integrated experimental–computational approaches for metallodrug–protein binding, particularly for Cu-based species. To do so, we used a previously Cu-based compound reported by our group, whose structure has been well-characterized and exhibited promising anticancer activity, as a practical case study (complex **C1**) [19–21]. Besides exhibiting biologically relevant redox activity and a remarkable reactive oxygen species (ROS)–mediated cytotoxicity, the solid state of the complex **C1** is constituted by a dimeric $[Cu(\mathbf{L1})]_2$ structure (**C1-i**), which equilibrates with the corresponding monomeric form (**C1-ii**) when dissolved in coordinating solvents such as dimethyl sulfoxide (DMSO) and/or H_2O (Scheme 1) [20]. **L1** binds the Cu(II) in a tridentated chelating fashion, whereas the fourth donor atom coordinates the metal center of the second molecular entity to form the dinuclear structure (dimer **C1-i**). The cleavage of the dimeric structure opens a coordination vacancy at the equatorial plane that can be occupied by a solvent molecule (**C1-ii**), thereby leading to a potentially more labile and reactive site for competing metal-binding moieties with higher affinity (e.g., amino acids of proteins).

In this study, we assessed the stability of the Cu(II) complex in a biologically relevant medium and evaluated coordinative and noncoordinative interactions between the metal complex and several relevant bloodstream and extra/intracellular proteins using experimental (spectroscopic/spectrometric) and computational methods (density functional theory [DFT] and protein–ligand docking for metallodrug binding site prediction) (Figure 1).

2. Results and Discussion

2.1. Stability of the Cu(II) Complex. Evaluation of the stability of the Cu(II) complex in biologically relevant media was carried out by electron paramagnetic resonance (EPR) spectroscopy in Dulbecco's modified Eagle's medium (DMEM). DMEM is composed of several salts (e.g., chlorides, sulfates, carbonates, and phosphates) and glucose, and it is supplemented with at least 13 amino acids, 8 vitamins, and phenol red for pH indication [22]. Therefore, it contains multiple potential competitor ligands for metal-containing species. The Cu(II) complex **C1** was dissolved in the media and incubated at 37°C for 24 h. The obtained EPR spectra at corresponding times ($t = 0$ h and $t = 24$ h) were compared to those obtained in DMSO solution as a reference (Figure 2 and Table 1).

The analysis of the spectrum in DMEM at $t = 0$ h reveals that there is a single Cu(II) center type, with $g_{//} > g_{\perp} > g_e$ and corresponding to an N_2O_2-donor square-planar or square-pyramidal-derived geometry around the Cu(II) [23–25]. The g and A tensors of the main species identified ($g_{//} = 2.246$, $A_{//} = 178{\cdot}10^{-4}\,\mathrm{cm}^{-1}$, $g_{\perp} = 2.049$) were not

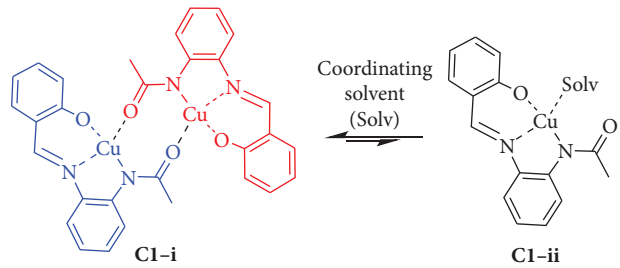

Scheme 1: Equilibrium for complex **C1** in coordinating solvents. Two species equilibrate, dimeric $[Cu(\mathbf{L1})]_2$, structure (**C1-i**), and its corresponding solvent-stabilized monomeric form (**C1-ii**) [20].

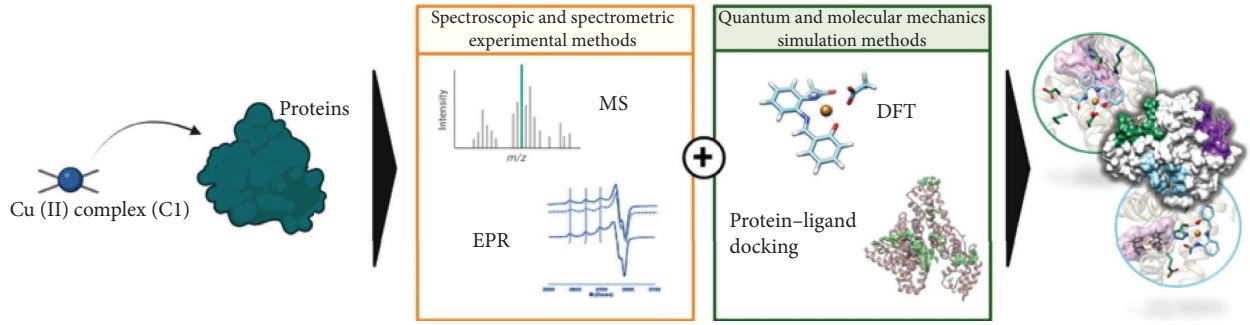

Figure 1: Integrating experimental–computational approaches to study copper (Cu)-based drug–protein interactions. Cytotoxic Cu(II) complex **C1** [20] was incubated with several relevant bloodstream and extra/intracellular proteins. Different spectroscopic (electron paramagnetic resonance [EPR]), spectrometric (mass spectrometry [MS]), and computational (density functional theory [DFT] and protein–ligand docking) methods were complementarily employed to profile the interaction with proteins. This figure has been designed using BioRender software.

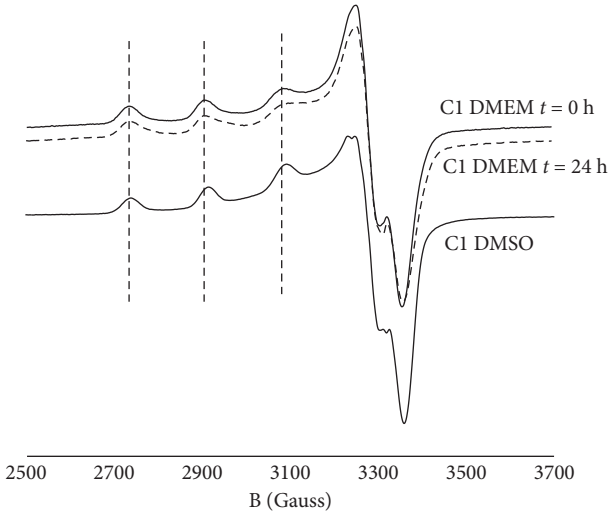

Figure 2: Stability assessment of the Cu(II) complex **C1** by EPR spectroscopy. X-EPR band (120 K) of **C1** in DMEM at $t = 0$ and after 24-h incubation at 37°C, compared to **C1** in DMSO [20].

altered concerning the reference ones, i.e., those of **C1** in DMSO (Table 1). Considering that g and A parameters are highly influenced by the changes in the metal coordination environment, especially on the first coordination sphere, these results indicate that **C1** in DMEM maintains the same (or analog) coordination core as in DMSO, which is assigned to the monomeric **C1-ii** species (NB: The dimeric structure [**C1-i**] in equilibrium is EPR silent) [20].

The lack of variation of the main g and A parameters over time, together with the minimal decrease in the EPR signal area for the main Cu(II) species, suggests that this Cu(II) structure (ascribed to the Cu(II) monomeric species **C1-ii**) is stable in the medium for at least 24 h, and it could be therefore one of the potential (re)active Cu-containing species of **C1**.

2.2. Interaction With Proteins. The interaction of the Cu(II) complex toward proteins was then evaluated using different experimental spectroscopic and spectrometric analytical techniques. Four model proteins (two high-molecular-weight [MW] proteins and two low-MW proteins) were selected because of their abundance, known metal-binding affinities, and biological relevance: HSA, Tf, Myo, and Cyt. HSA and Tf are relevant high-MW bloodstream proteins that any metallodrug will encounter upon intravenous administration, with HSA being among the most abundant ones [26, 27]. Myo is a low-MW heme protein found in humans in the bloodstream after muscle injury, and it acts as a model for hemoglobin, a highly present protein in red blood cells [28, 29]. Cyt, in turn, is also a small (low-MW) heme protein associated with the internal membrane of mitochondria. Despite not being present in the bloodstream, it was selected as a relevant model of intracellular proteins,

Table 1: EPR parameters for the Cu(II) species identified in cell culture media stability evaluation.

EPR incubations	$g_{//}$	$A_{//}$ (cm^{-1})	$g_{\perp}$	$A_{\perp}$ (cm^{-1})	$g_{//}/A_{//}$ (cm)	Proposed coordination[a]
C1 (DMEM)	2.246	$178{\cdot}10^{-4}$	2.049	$< 30{\cdot}10^{-4}$	126	N_2O_2
C1 (DMSO) [20]	2.244	$183{\cdot}10^{-4}$	2.043	$< 30{\cdot}10^{-4}$	122	N_2O_2

Note: The values of the species observed from the dissolution of complex **C1** in DMEM are compared to the corresponding values in DMSO (Figure 2). The ratio between $g_{//}$ and $A_{//}$ EPR parameters is indicative of the planarity of the structure ($g_{//}/A_{//} < 140$ cm, for structures with no or little distortion from planarity).

[a]The Cu(II) coordination environment (donor atoms) was determined based on an established empirical correlation [23–25].

with a largely conserved amino acid sequence between different species and a crucial role in intracellular redox cell respiratory processes [30].

Electrospray ionization mass spectrometry (ESI-MS) was used to identify protein–metallodrug adducts (Figure 3). Before the incubation with the Cu(II) complex **C1**, the four native proteins were characterized by MS to confirm the absence of any interfering species and to find out their experimental MW following previously reported conditions [31, 32]. Within the explored m/z working range, several ionization states were observed. The experimental values determined by ESI-MS were 66,558 Da for HSA, 78,017 Da for Tf, 17,567 Da for Myo, and 12,360 Da for Cyt (Figure S1 and Table S1). Several species were identified in Tf and HSA cases, including different glycosylated or acetylated forms (frequently observed in purified Tf [33]). A single species was mainly detected in the ESI-MS spectra for the proteins with the lowest MW (Myo and Cyt).

Proteins were first incubated with complex **C1** at 37°C for 24 h, at a fixed (protein:**C1**) molar ratio of 1:2, and then analyzed via ESI-MS. The results showed that **C1** interacted with almost all the studied proteins (Figure 3). Interestingly, a different behavior of **C1** toward each of the highest MW proteins (HSA and Tf) was observed (Figures 3(a) and 3(b)). Although for Tf no interaction could be concluded from the ESI-MS at the assayed (protein:**C1**) ratio, the analysis for HSA indicated a clear interaction with the Cu(II) complex, with several peaks at the different charge states that could be attributed to adducts of the protein with different **C1** species. The amplification of the m/z region corresponding to the charge states +38 and + 39 of HSA showed that these adducts were constituted by one and two entities of **C1** per unit of protein (or two and four, respectively, if considering a nonsolvated tricoordinated monomeric form of **C1** ([Cu(**L1**)], **C1-iii**)). It is well known that Cu(II) strongly interacts with albumin to form stable albumin–Cu(II) adducts, with the metal bound to different external and internal binding sites of HSA, such as the multimetal-binding site (MBS) and the ATCUN motif [34, 35]. HSA could, therefore, promote **C1-i** cleavage or **C1-ii** solvent exchange and subsequent Cu(II) coordination by protein amino acids. Yet, despite the high Cu(II)-binding affinity for HSA, MS data show that **C1** partially preserves its structural integrity upon HSA binding.

The MS analysis of the complex **C1** with the smaller proteins, Cyt and Myo, also revealed significant interaction (Figures 3(c) and 3(d)). First, a substantial decrease in the peak intensity corresponding to the native protein was observed (both +6 and +7 charge states). In both cases, peaks corresponding to adducts of the protein with a monomeric form **C1** were identified. Both Myo and Cyt sequences have several coordinating amino acids with affinity for Cu(II), such as histidine (His) [36], which could promote the cleavage of the dinuclear structure **C1-i** upon protein binding. The generated Cu(II) equatorial coordination vacancy in **C1-iii** could then be occupied by any of the binding amino acids of the protein. Moreover, adducts corresponding to the protein and (fragments of) **L1** were also observed, supporting a possible partial decoordination of **L1** from the Cu(II) metal center due to competition with coordinating amino acid residues of the proteins.

Overall, the data set obtained by MS confirmed the binding of **C1** to almost all tested proteins, except Tf. To better understand both the mode of binding and the nature of the different species formed, complementary EPR experiments were performed. The EPR technique has become increasingly common in the characterization of interactions between paramagnetic metal complexes and proteins as the coordination of the Cu(II) at the equatorial plane by amino acid side chains generally results in characteristic EPR signals [24]. Given the impact of bloodstream proteins on metallodrug biodistribution and eventual efficacy, the EPR analyses were focused on the two bloodstream proteins that showed positive interaction with **C1** in previous MS experiments, namely HSA and Myo (which also act as high- and low-MW model proteins, respectively).

EPR analyses were carried out 24 h after incubating the different proteins with **C1** in PBS-containing media at physiological pH and 37°C. For HSA, the study of the EPR spectrum revealed two main Cu(II) center types in solution (Figure 4(a)), both with $g_{//} > g_{\perp} > g_e$, and therefore assigned to square-planar or square-pyramidal-derived geometries (Table 2) [23–25]. These two Cu(II) species have rapid formation kinetics as they are observed just after mixing the protein with the complex ($t = 0$ h; Figure 4(a)) and remain stable for at least 24 h (see $t = 24$ h; Figure 4(a)). One of the EPR set of signals (Species 1; Figure 4(a) and Table 2) corresponds to a Cu(II) center in square-planar or square-pyramidal geometry with N_2O_2-donor coordination environment, with EPR parameters highly similar to those found for **C1** dissolved in DMSO and in DMEM (namely $g_{//} = 2.246$, $A_{//} = 178{\cdot}10^{-4}\,cm^{-1}$, and $g_{\perp} = 2.049$) (Table 2). Consequently, Species 1 can be structurally related to monomeric **C1**. The minor changes on the g and A parameters compared to the features of **C1** in DMSO suggest an N_2O_2 coordination sphere in Species 1, as in **C1-ii**. The slight

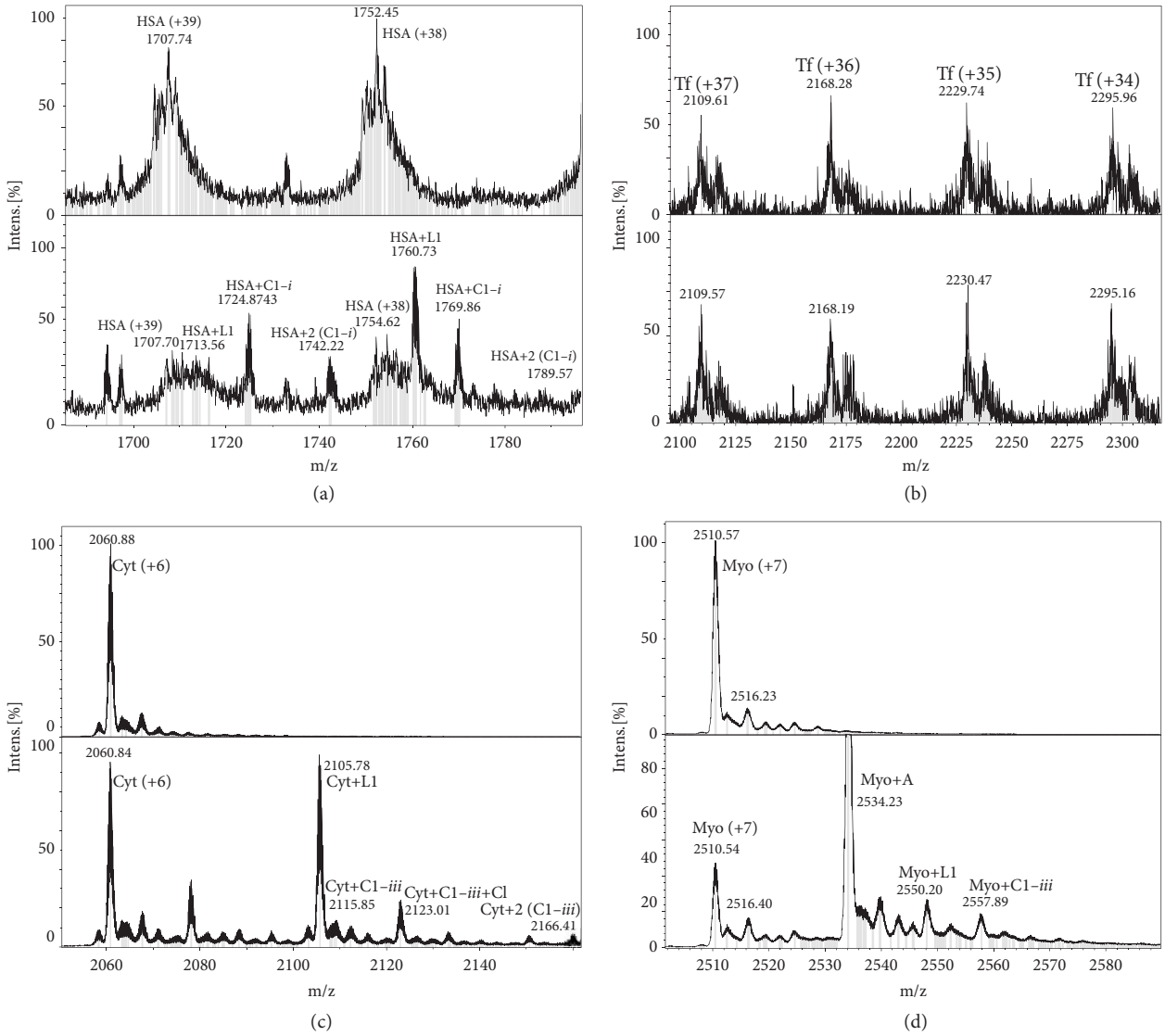

FIGURE 3: Evaluation of protein interactions by electrospray ionization mass spectrometry (ESI-MS). Protein–Cu(II) complex **C1** (1:2 molar ratio) incubations for 24 h at 37°C studied by ESI-MS. (a) HSA–**C1** interactions at the region m/z 1680–1800 (+39 and +38 charge states), (b) Tf–**C1** interactions at the region m/z 2100–2350 (+34 to +37 charge states), (c) Cyt–**C1** interactions amplified at the region m/z 2050–2170 (+6 charge state), and (d) Myo–**C1** interactions amplified at the region of 2500–2590 (+7 charge state). For the peak [Myo + A] in (d) (m/z 2534.23), "A" could be related to *N*-(2-aminophenyl)acetamide ($C_8H_{10}N_2O$), a fragment from **L1**. *Note:* "**C1-iii**" (in (c) and (d)) refers to the tricoordinated monomeric unit of the complex **C1** (i.e., [Cu(**L1**)]), and every "**C1-i**" in the peak assignments for HSA (in (a)) would equally fit as "2(**C1-iii**)."

modification could arise from the binding of either a solvent molecule (DMSO or H_2O from DMEM) or O-donor amino acids as long as it does not cause a major structural change around the Cu(II) center [37–40]. The second Cu(II) center identified in the EPR spectral analysis (Species 2; Figure 4(a)) has a lower $g_{//}$ value ($g_{//} = 2.18$; Table 2), which points to a higher *N*-donor contribution in the Cu(II) coordination sphere, i.e., leading to a Cu(II) *N*-donor-rich species (N_3O- or N_4-donor atoms in the equatorial plane) (Table 2) [23–25]. The spectral features are consistent with those found upon binding of HSA to Cu(II) ions (Figure 4(a)) and could thereby be ascribed to the Cu(II) coordination by the ATCUN motif of HSA [34, 35]. Altogether, EPR data corroborate that although **L1** can be partly dissociated from the metal center, monomeric entities are preserved upon protein binding and could interact with albumin on surface binding sites and/or within the protein cavities.

Regarding Myo, incubation of **C1** with the protein revealed an analogous EPR spectrum to **C1** in DMSO/DMEM, with mainly one Cu(II) center type that was stable also after 24 h in the presence of Myo (Table 1 and Figure 4). Low-field EPR spectrum showed the characteristic Myo signal of the high-spin Fe(III) center ($S = 5/2$) of the heme group in an axially symmetric environment characterized by two resonances: the first at $g_{\perp}^{\text{eff}} = 6$ and a broader one at $g_{//}^{\text{eff}} = 2$ (Figure 4(b)) [41]. Incubation of the protein with **C1**

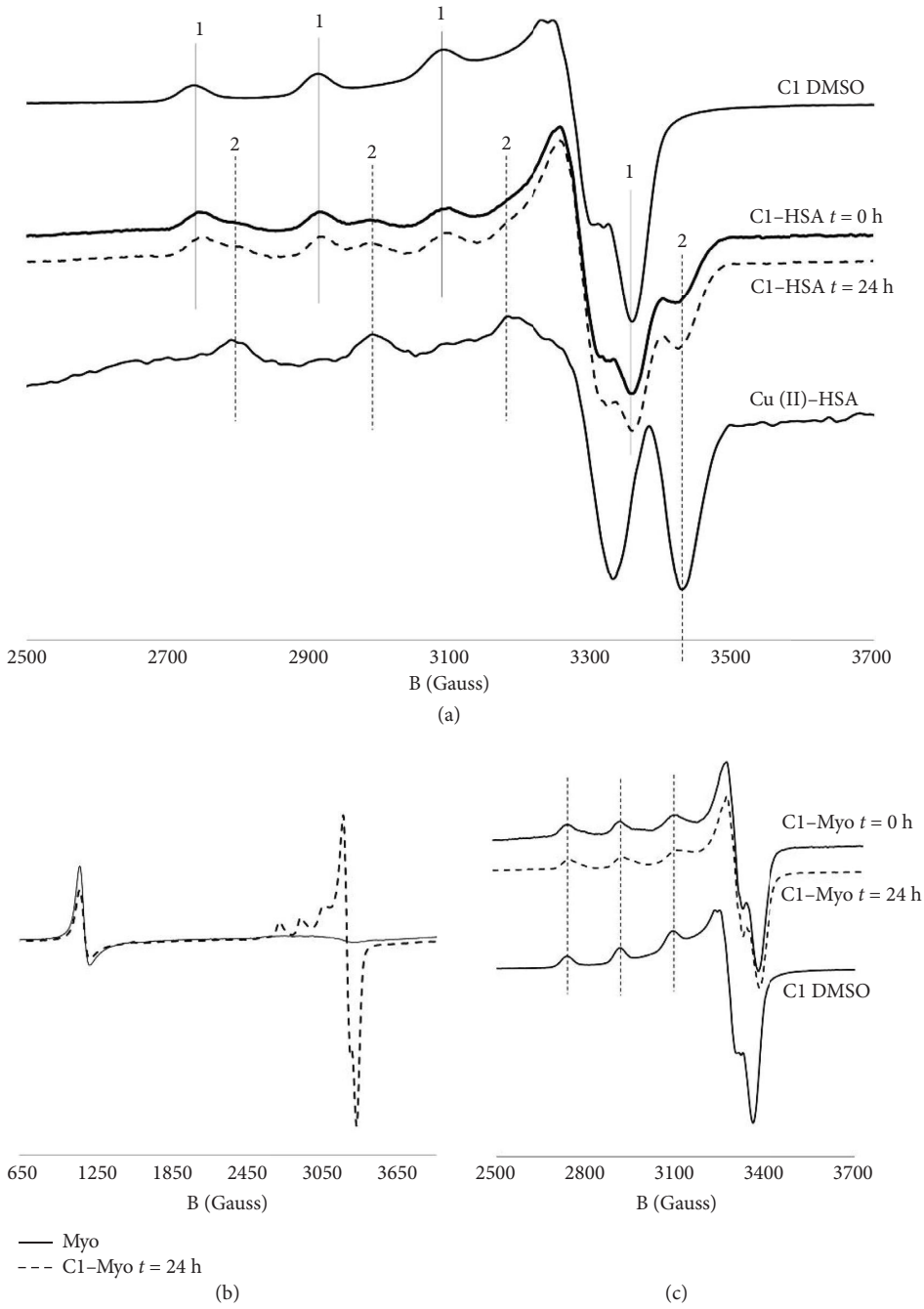

Figure 4: Evaluation of protein interactions by EPR spectroscopy. Electron paramagnetic resonance (EPR) band spectra (120 K) of the samples of **C1** incubated with (a) HSA (where signals assigned as (1) and (2) indicate the two identified Cu(II) center types) (Species 1 and 2, respectively); (b–c) incubated with Myo with (c) magnification on the region of the Cu(II) signal.

did not induce any significant change on the Fe heme site of the protein, thus pointing to the binding of **C1** at a Myo site not related to the heme active pocket. No significant changes were observed in the EPR parameters of Cu(II), indicating no substantial changes in the Cu(II) coordination sphere in **C1** between free and protein-bound forms. Several phenomena could explain the EPR data. On the one hand, the interaction of the metallodrug may occur in the form of intermolecular interactions between **C1** and the protein, with the **C1** structure intact upon binding. On the other hand, and considering current knowledge on Cu–protein interactions in the Protein Data Bank (PDB), the solvent in **C1-ii** could be potentially exchanged by an *O*-donor coordinating amino acid residue from the protein, possibly glutamate (Glu) or aspartate (Asp) or even one oxygen atom from a backbone amide group. As no major influence is observed on the EPR values as compared to **C1** in DMSO, it is reasonable to believe that the newly formed Cu-O bond

Table 2: EPR parameters for the Cu(II) species identified in the presence of HSA and Myo.

Sample	$g_{//}$	$A_{//}$ (cm^{-1})	$g_{\perp}$	$A_{\perp}$ (cm^{-1})	$g_{//}/A_{//}$ (cm)	Proposed coordination (donor atoms)[a]
HSA–C1						
Species 1	2.246	$178{\cdot}10^{-4}$	2.049	$< 30{\cdot}10^{-4}$	126	N_2O_2
Species 2	2.180	$204{\cdot}10^{-4}$	2.040	$< 30{\cdot}10^{-4}$	107	N_3O/N_4
Myo–C1	2.246	$178{\cdot}10^{-4}$	2.049	$< 30{\cdot}10^{-4}$	126	N_2O_2
C1-ii (DMSO) [20]	2.244	$183{\cdot}10^{-4}$	2.043	$< 30{\cdot}10^{-4}$	122	N_2O_2

Note: EPR parameters were obtained from the analysis of the HSA–**C1** and Myo–**C1** spectra shown in Figures 4(a) and 4(c) and compared with the corresponding spectrum of **C1** in DMSO, that is, **C1-ii**.

[a]The Cu(II) coordination environment (donor atoms) was determined based on an established empirical correlation [23–25].

would still be weak and that, in all cases, the protein binding does not imply structural/geometric changes in the Cu(II) compound.

Overall, EPR experimental data confirmed the interaction of the Cu(II) complex with HSA and Myo, supported by the observation of several protein–metal complex adducts by MS. Although EPR analyses, in the presence of proteins, allowed the identification of different Cu(II)-containing species and their possible coordination environments (donor atoms), the intrinsic limitations of both experimental methodologies (MS and EPR) required the use of complementary computational methods to achieve the molecular description of the binding modes and sites.

2.3. Computational Insights Into Protein Complex Interactions. To further understand the nature of the interactions of **C1** with proteins, DFT calculations were first performed. HSA and Myo were again selected as the most representative proteins to be computed. As for the experimental section, the three main structural models for **C1** were used for the calculations: (a) dimeric, **C1-i**; (b) monomeric **C1-ii**, with a solvent molecule (DMSO/H_2O) coordinated in the equatorial plane; and (c) **C1-iii**, monomeric structure with the Cu(II) tricoordinated center (Figure 5). From a computational point of view, tetracoordinated Cu(II) centers in **C1-i** and **C1-ii** cannot present further coordination at the equatorial plane. Hence, only axial binding and other weaker interactions at the level of the second coordination sphere were considered, while structure **C1-iii** can form direct metal coordination bonds with different donor residues of the proteins. Besides, all three can also physically interact with proteins via hydrophobic and polar interactions.

DFT-based EPR simulations were performed and compared with experimental EPR spectra to provide insights into the nature of the first metallic coordination sphere upon protein binding. DFT calculations were initially performed on small models (clusters) [42] surrounding the EPR-active **C1-ii** and **C1-iii** forms. These consisted of monomeric **C1-iii** and His and Asp/Glu amino acids as coordinating models. The results found were compared to the data obtained with solvent-coordinated **C1-ii**. Dimeric tetracoordinated Cu(II) structure **C1-i** was not evaluated due to its reported EPR silent nature [20]. To simulate the binding functional groups for His and Asp/Glu, two simplified models were first assembled by computing an imidazole (Cu-N) and acetate (Cu-O) groups, respectively (Figure 6). The systems were optimized considering divalent Cu(II) with a d^9 electronic configuration with a single unpaired electron and a nuclear spin of 3/2. After optimization of the structures, a square-planar-derived geometry with a slight distortion from planarity was obtained in all cases (Table 3), in accordance with the previous experimental EPR values (Table 2). Additionally, square-pyramidal geometries were explored by placing H_2O and DMSO in the upper and lower axial positions of the imidazole and acetate **C1-iii** models, followed by EPR calculations. The results indicate that these pyramidal models differ from the experimentally obtained values (see SI for details; Figure S4 and Table S6).

DFT-calculated EPR data showed no significant differences between the EPR parameters in the different **C1** binding models, with one exception: through EPR simulations, the only Cu(II) species that could be confidently identified by comparing the simulated-versus-experimental EPR values was ascribed to the Cu(II)–ATCUN binding (Table 3), namely *Species 2* in the experimental EPR data of **C1**-HSA (see Table 2). These findings confirm the high Cu(II) binding capacity of HSA, whose ATCUN binding site competes with **L1** to coordinate Cu(II) and promotes partial decoordination from the metal complex.

According to the calculated EPR parameters, the Cu(II) in **C1-ii** and **C1-iii** could either (*a*) maintain a solvent molecule (H_2O or DMSO) as the fourth equatorial ligand (Cu-O bond, i.e., **C1-ii**) and interact with the protein through purely nonbonded intermolecular interactions or (*b*) be coordinated by His (Cu-N bond) or Glu/Asp (Cu-O bond) residues (i.e., **C1-iii**–imidazole or **C1-iii**–acetate) together with hydrophobic interactions of the rest of the complex with the protein. The complexity of the system and the similarities between all the computed values impair the accurate determination of any other HSA/Myo-bound **C1** species besides Cu(II)–ATCUN solely via EPR calculations, and therefore, the exploration of protein receptor topology becomes crucial.

Protein–ligand docking calculations were performed to answer this question. This type of calculation is becoming an asset for estimating the relevance of possible interactions of metal-containing molecules (commonly referred to as metalloligands in docking) with proteins. This has been possible thanks to new scoring functions that allowed considering both active (formation of coordination bonds between the metal in the complex and the protein) and inert

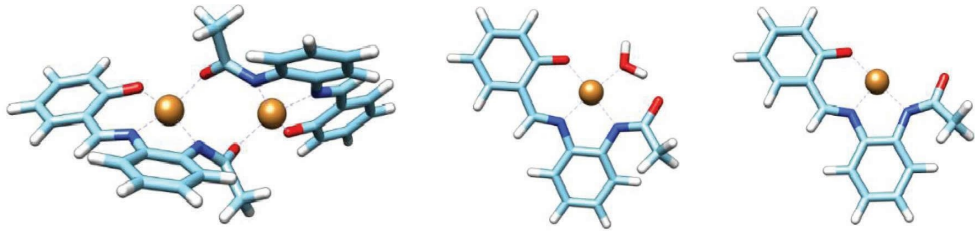

FIGURE 5: Representation of the Cu(II) structural models used to perform DFT and docking calculations with the complex **C1**. Three structural forms of the Cu(II) complex **C1** were considered for computation: (a) **C1-i** dimeric form, (b) **C1-ii** monomeric form coordinated by a solvent molecule (water), and (c) **C1-iii** monomeric form with a coordination vacancy at the equatorial plane.

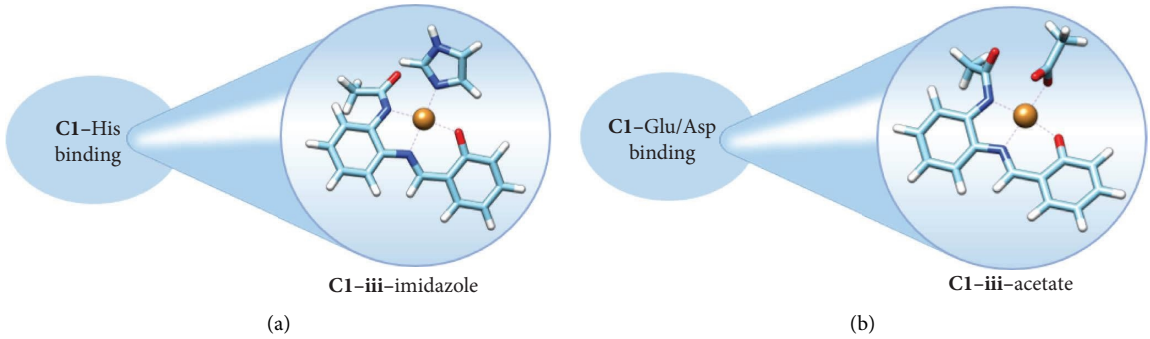

FIGURE 6: Cu(II) coordination models used for the Cu(II) complex–amino acid DFT-based EPR simulations. (a) **C1**–His binding, simplified by a **C1-iii**–imidazole coordination model system. (b) **C1**–Glu/Asp binding, simplified by a **C1-iii**–acetate coordination model system.

TABLE 3: Computational EPR data for the **C1** complex.

Cu(II) structure	Donor atom[a]	Species	$g_{//}$	$A_{//}$ (cm^{-1})	$g_{\perp}$	$A_{\perp}$ 10^4 (cm^{-1})
C1-ii	Cu-O	**C1-ii** (DMSO)	2.200	$154{\cdot}10^{-4}$	2.049/2.076	13/42
		C1-ii (H_2O)	2.178	$199{\cdot}10^{-4}$	2.052/2.058	7/10
C1-iii	Cu-O	**C1-iii**–acetate	2.177	$189{\cdot}10^{-4}$	2.050/2.053	4/9
	Cu-N	**C1-iii**–imidazole	2.186	$188{\cdot}10^{-4}$	2.050/2.067	7/11
Cu(II)–ATCUN	Cu-N	Cu(II)–ATCUN	2.135	$204{\cdot}10^{-4}$	2.041/2.042	15/20

Note: EPR parameters for monomeric **C1-ii** and **C1-iii** (see Figure 5) coordinated to solvent and to imidazole or acetate groups. The dimeric structure **C1-i** is EPR silent [20] and, therefore, not computed. Cu(II)–ATCUN is added for comparison.
[a]For all **C1**-related structures, this refers to the fourth donor atom around the Cu(II) metal center. The three other donor atoms to complete the tetra-coordinated Cu(II) structure correspond to *N*, *N*, and *O* (provided by **L1**). For the Cu(II)–ATCUN, the four donor atoms are *N*, from the amino acid residues of the ATCUN site [34, 35].

(no coordination bond formed between both species) binding modes [43].

In this study, protein–ligand dockings were carried out on Myo and HSA using the software Gold v5.2 [44] with the scoring function GoldScore optimized for dealing with metalloligands [45]. Because of the differences in size and topology between Myo and HSA, slightly different protocols were applied to each system. Myo has a compact structure as a globin, with only one cavity corresponding to the heme binding site. In this case, blind docking was performed, followed by more accurate calculations in the best binding regions identified. However, HSA is a large protein known to present many internal cavities, which leads to blind docking calculations providing a high number of solutions and nonconverged results.

To help in finding the valid cavities for the binding of **C1** in both Myo and HSA, blind dockings were combined with calculations of relative solvent-excluded surface area (relSESA), which allows the identification of compatible cavities (Tables S3 and S4). If found, dockings were repeated specifically in these spaces.

For Myo, docking calculations highlighted three potential surface binding sites for **C1**: **A**, **B**, and **C** (Figure 7 and Table S2). GoldScore *max. fitness* values at these sites vary from ca. 35 to 55 units, showing a reasonable binding propensity for the protein:**C1** adducts (Table S2). In general,

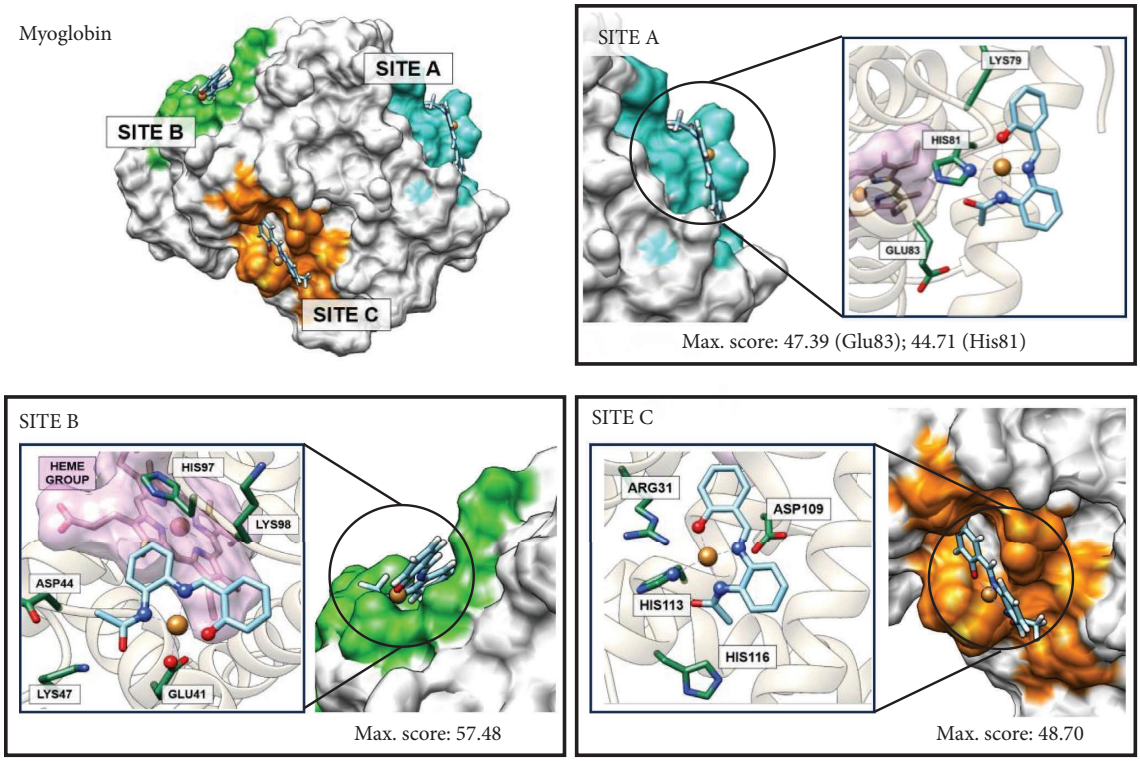

FIGURE 7: Docking evaluation for C1 interactions with myoglobin. Myoglobin (Myo)–**C1** docking calculations to predict protein binding sites. Sites **A**, **B,** and **C** exhibit the best docking poses, and the protein environments and scoring (fitness) values where **C1** binds through direct metal coordination **C1-iii** are represented (zoomed-in). The purple-colored surface displays the heme group.

solutions where amino acids coordinate Cu(II) present better scoring values than any interactions of a non-coordinative nature or at the level of the second coordination sphere, such as for **C1-i** or **C1-ii**. The general tendency of predicted affinities is **C1-iii** > **C1-i** > **C1-ii**, showing that the preferred binding mode is direct Cu(II) coordination of the monomeric **C1-iii** with the protein. However, nonnegligible contributions to noncoordinative interactions between **C1-i** and Myo are present. Different tendencies are observed between sites **A**, **B**, and **C** (Figure 7 and Table S2). Site **C** is the least discriminative regarding interactions between **C1** and Myo as *fitness mean* values do not exceed seven units difference (between 41 and 48 GoldScore units). Thus, dockings suggest that any form of the **C1** could interact at this site. If the fourth position of the coordination sphere becomes vacant, the protein could coordinate the metal with one of three amino acids in the preferential order His113 > Glu105 ≈ Asp109 (Table S2). For the other two sites, **A** and **B**, **C1-ii** appears to be the worst binder concerning **C1-i** and **C1-iii**. This could be explained in general by physicochemical terms as **C1-i** has a higher MW that promotes higher scoring throughout hydrophobic interactions, whereas **C1-iii** presents a direct coordination with the metal that increases fitness. For site **A**, **C1-iii** presents the best fitness with metal coordination with His81 or Glu83, although the low difference in scoring (less than 3 GoldScore units) does not allow to discriminate between both binding modes. For site **B**, the same tendency is observed. However, the best binding solution is observed for **C1-iii** with the coordination of Glu41, and this solution is suggested to be the preferential binding mode for **C1** to Myo. Because previous experimental studies showed the presence of the dimeric **C1-i** form in solution [20], its interaction with Myo cannot be discarded. It is essential to highlight that the preferred predicted binding mode for **C1-i** is also site **B** (51 units). As a final remark on this system, it is interesting to comment that none of the amino acids predicted to coordinate the Cu(II) ion are anchored deeply inside the protein scaffold (Table S3). Altogether, this part of the study suggests that all binding sites could contribute to the total amount of interactions of the protein with **C1**.

Because of its size, blind protein–ligand dockings in HSA are challenging, so the strategy to identify **C1** binding modes consisted of first identifying binding sites and then performing protein–**C1** dockings on those sites. The former was done in two steps: (1) the search for accessible binding sites on the protein surface using solvent-accessible descriptors (USCF Chimera software [46] using the relSESA method proposed by the Murgita group [47]; Table S4) and (2) the search for small molecule internal binding sites using the reported crystallographic structure of HSA containing trapped octadecanoic acid (ODA) molecules as a reference [48]. Seven distinct inner cavities (internal sites) were identified, each assigned to a numerical description from 1 to 7 (Figure S2). For subsequent dockings of **C1** in HSA, ODA molecules were removed from the X-ray structure.

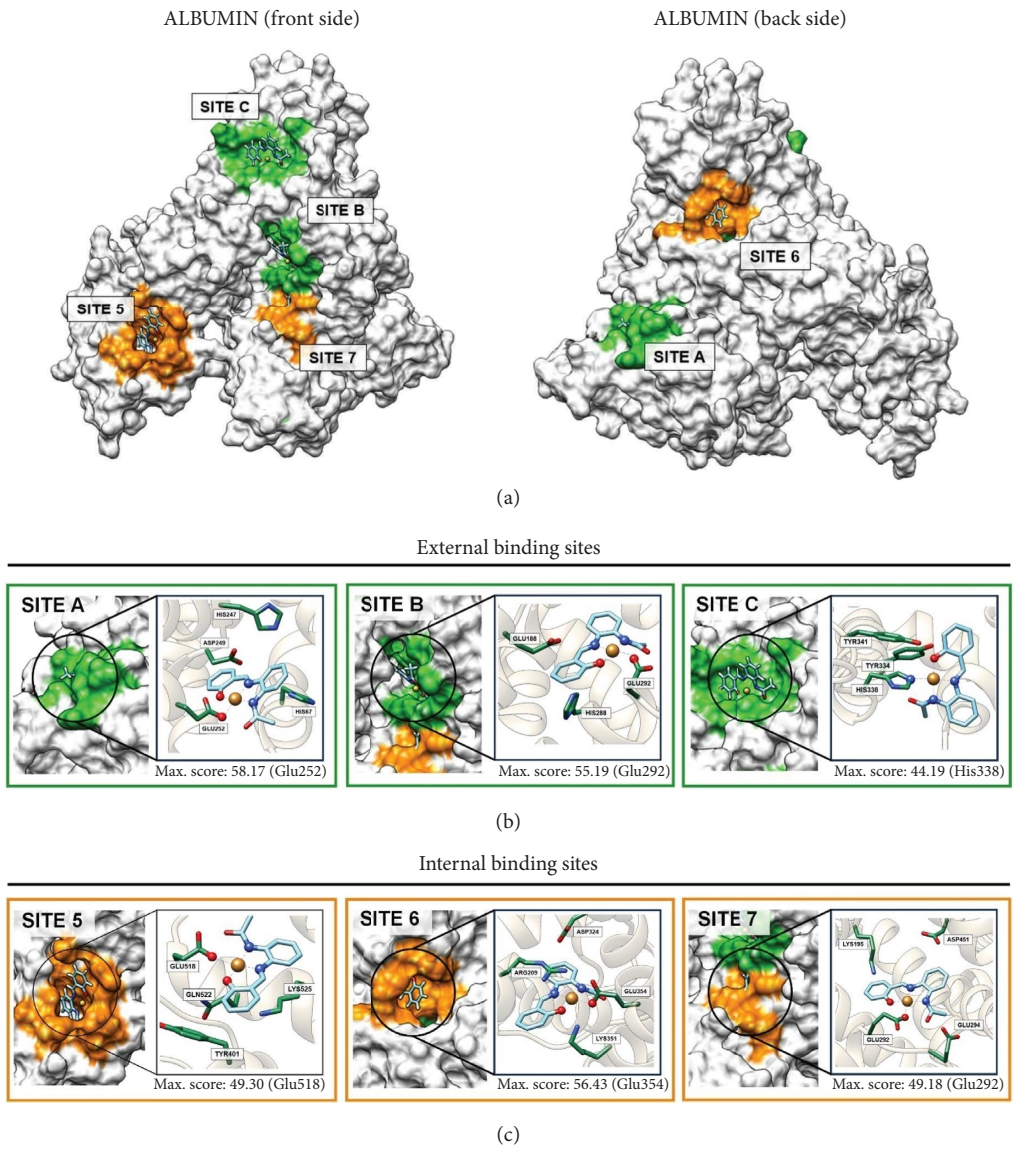

Figure 8: Docking evaluation for Cu(II) complex with albumin. Human serum albumin (HSA)–**C1** docking calculations to predict protein-binding sites. (a) Front and back side images of albumin are represented along the best docking positions. The green-colored surfaces (Sites **A**, **B,** and **C**) correspond to external coordination positions found by the relSESA method (Table S3). The orange-colored surfaces (Sites 5, 6, and 7) represent the inner cavity coordination sites found by the fatty-acid approach study. Zoom-in representation of the best docking poses (and scoring values) of the binding of Cu(II) in **C1** to HSA amino acid residues in (b) outer surface binding sites and (c) inner cavities.

Solutions of the docking experiments for **C1** species to HSA are illustrated in Figure S3, and the best poses are summarized in Table S5 and depicted in Figure 8. All docking solutions predicted binding values in a narrow range of magnitudes, from 42 to 59 units (*fitness max.* values; Table S5). Among the seven internal sites available in the protein scaffold, based on scoring, three sites are preferred, namely 5, 6, and 7 (Figure 8(c) and Table S5). The internal cavities only allow good affinities for **C1-ii** and **C1-iii** as the dimeric species **C1-i** is energetically unfavored because of their larger size and steric impairments.

Regarding interactions with HSA at the protein surface (external cavities), three sites with good predicted binding affinities were identified (namely **A**, **B**, and **C**; Figure 8(b) and Table S5). Calculations pointed to an overall preferential binding of Cu(II) in **C1** to Glu or His residues, with scoring values of 58.17 for Glu252 (site **A**) and 55.19 for Glu292 (site **B**). Although the preference at sites **A** and **B** for Glu amino acids may contrast with the higher affinity for His coordination predicted at site **C** (His338), the latter showed a lower scoring value (44.19). Despite the intensive work at the frontline of the current framework in predicting the

interaction of metallic species with proteins by computational means, the final discrimination between these remaining sites and the predominant form of interaction cannot be reached.

Altogether, our computational study points to a good affinity of **C1** for proteins, mostly through direct Cu(II)–protein binding of the monomeric species and preferentially via Glu(/Asp) residues (Cu-O binding). Interactions with *N*-donor amino acid residues (e.g., His) were also observed, but with a lower probability. Overall, no single, specific binding mode or site can be univocally assigned, suggesting a non-specific interaction of the **C1** compound with the proteins. However, three main surface areas in both Myo and HSA, as well as three internal cavities for HSA, were identified to more preferentially accommodate **C1** (which could potentially also host other metallodrugs, as we observed previously for V drugs) [49, 50]. Importantly, although experimental data showed that HSA can partly degrade the Cu(II) complex and bind free Cu(II) ions due to the high metal-binding affinity of the ATCUN motif, docking calculations also showed that in line with MS and EPR experimental data, the Cu(II) coordination structure remains partly preserved after protein binding.

3. Conclusions

Here, we report a combined experimental–theoretical study of the interaction of a Cu-based metallodrug with several model proteins that could be relevant to understanding its biological performance. To do so, the systems selected were, on the one hand, a Cu(II) *N*,*N*,*O*-chelated salphen-like metal complex and, on the other hand, several relevant bloodstream and intracellular proteins, including HSA, Myo (as a model of hemoglobin), Tf, and Cyt. MS and EPR spectroscopy were used to identify **C1**–protein species. MS data showed that the metal complex **C1** interacts with HSA, Myo, and Cyt, based on the presence of several peaks corresponding to adducts of **C1**-related species with the different proteins. Experimental EPR data of the Cu(II) complex with HSA and Myo pointed to structural preservation of the metallic surrounding upon protein binding and a preferential N_2O_2-donor coordination environment around the Cu(II). Further insights into the protein-binding modes and sites were obtained first by DFT calculations. For this, small cluster models where the metal could be bound to prototypical Cu-binding amino acids (e.g., His and Glu) were employed. These calculations were used to simulate EPR data and compare them with the experimental EPR results. Only the Cu(II)–ATCUN adduct could be identified at this stage, and no other EPR signals were univocally attributed. Therefore, protein docking methods were applied to account for the full dimensions of both Myo and HSA, and surface and inner cavities were scanned. The best scoring values were primarily obtained for direct coordination of the metal of **C1** to *O*-donor amino acid residues of the proteins (mostly Glu). However, noncoordinative interactions between dimeric **C1** and the proteins were also observed to be relevant and worth considering.

This study highlights how the development of modeling frameworks for bioinorganic systems in combination with experimental techniques allows further characterization of metallodrug–protein interactions and can contribute to the understanding of metallodrug speciation and its targets in biological systems. This can eventually help in the prediction of therapeutic performance and assist in the design of more effective metallodrugs.

4. Experimental and Computational Section

4.1. Materials and Reagents. Proteins (HSA, Tf, Myo, and Cyt C) were purchased in lyophilized (powder) form from commercial suppliers. NH_4HCO_3, DMEM (cell culture medium), glycerol, and DMSO were also obtained from commercial sources and used as received. Complex **C1** was resynthesized following previous protocols [20]. **C1** characterization fits well with previously reported data.

4.2. Experimental Methods

4.2.1. EPR Spectroscopy. EPR measurements were carried out on a Bruker ELEXSYS 500 X-band CW-ESR spectrometer, with an ELEXSYS Bruker instrument equipped with a BVT 3000 digital temperature controller. The spectra were recorded at 120 K in frozen DMSO or DMEM solutions (containing 5%–10% DMSO to solubilize **C1**), otherwise noticed. Typical acquisition parameters were as follows: microwave power of 10–20 mW, modulation frequency of 100 kHz, and modulation gain of 3 G. Simulations were performed using the EasySpin toolbox developed for MATLAB (Stoll & Schweiger, 2006).

To study Cu(II) speciation of **C1** in DMEM by EPR, stock solutions of **C1** in DMSO were diluted in DMEM (containing a maximum of 5% DMSO in the final solution). The samples were incubated for 24 h at 37°C, then 50% diluted with Milli-Q water containing 33% glycerol, and frozen using liquid nitrogen before EPR measurements. Protein–**C1** complex EPR measurements were performed after incubating the corresponding complex **C1** with the protein at a 1:1 molar ratio for 24 h at 37°C in a physiological medium (DMEM containing a maximum of 5% of DMSO to solubilize complex **C1**). Similar to before, incubated **C1**–protein samples were then diluted with Milli-Q water containing 33% glycerol and frozen in liquid nitrogen before EPR measurements. For the $t = 0$ h samples, aliquots of the **C1**–protein solutions were diluted with 33% glycerol in water and frozen immediately after preparation.

4.2.2. Mass Spectrometry. Protein complex interactions by ESI-MS spectrometry were carried out at the *Servei d'Anàlisi Química* (UAB) in positive mode and following a reported procedure in our group [31, 32]. Then, 20 mL of each sample was injected at 40 mL·min^{-1}; the capillary counter electrode voltage was 4.5 kV; the desolvation temperature was 100°C; dry gas was supplied at 6 L·min^{-1}. Spectra were collected throughout an m/z range from 800 to 3500. The liquid carrier was an ammonium acetate solution at pH 7 in water/

acetonitrile (85:15). Stock solutions of the proteins were freshly prepared for each experiment. **C1**–protein samples were prepared by incubating the corresponding complex with the protein at the specific molar ratio for 24 h and 37°C in 25 mM NH_4HCO_3 (pH 7.2), containing a maximum of 5% of DMSO to solubilize the complex **C1**.

4.3. Computational Methods

4.3.1. System Setup. For all the analyzed coordination compounds, GaussView 5.0 [51] was used to manually create and modify structures due to the lack of available crystallographic adducts of these small protein–ligands. Subsequently, geometry optimizations and harmonic frequency calculations were conducted using Gaussian 16 [52] at the DFT level. The hybrid Becke three-parameter B3LYP functional [53, 54] coupled with Grimme's D3 dispersion correction [55] was applied, complemented by the split-valence Pople basis set 6–31g(d,p) for the primary group elements [56]. For Cu, the Stuttgart–Dresden (SDD) basis set [57], incorporating f functions and pseudopotentials, was employed. It is worth noting that these computational settings have previously proven their efficacy and applicability in predicting the geometries of first-row transition metal complexes, as documented in the literature [58, 59]. An in-depth benchmarking was performed comparing the B3LYP and WB97XD functionals, with no significant differences observed in the geometries (see SI, Figure S5, and Table S7). The resulting structures of complexes **C1-i**, **C1-ii,** and **C1-iii**, including their respective atomic coordinates, were stored in .mol2 files, along with their molecular charge distribution data for the ongoing method implementations. For the calculations involving protein–ligand interactions, XRD structures of Myo (code: 4DC8) [60] and albumin (codes: 1AO6 [61] and 1E7I [48]) were taken from the PDB. These protein structures underwent preliminary processing, involving the removal of unwanted small molecules and crystallographic waters. Hydrogen atoms were subsequently added to the structures using USCF Chimera software [46], whereas the protonation states of amino acid side chains were determined through the PROPKA algorithm [62].

4.3.2. EPR Parameter Calculations. The g and A tensors for the Cu center in each complex were computed using the ORCA 5.0 software [63, 64], employing a method specifically developed and integrated into the software package for this purpose. The A tensor was obtained as a sum of the three contributions: the isotropic Fermi contact (A^{FC}), the anisotropic dipolar ($A^{D}_{x,y,z}$), and the spin–orbit (SO) coupling term ($A^{SO}_{x,y,z}$). To ensure precise estimations of A^{FC}, the calculations incorporated the unrestricted Kohn–Sham (UKS) formalism, considering the appropriate spin polarization. For the computation of EPR parameters, two distinct exchange and correlation functional combinations were employed: the generalized gradient approximation (GGA) PBE0 functional [65] and the B3LYP hybrid density functional [53, 54]. This protocol has consistently delivered the most accurate results in predicting electron paramagnetic spectra for Cu(II) coordination complexes [42]. In particular, g tensors were computed using the PBE0 functional, whereas Az values were obtained with the B3LYP functional. Both functional calculations used the identical Pople basis set, 6–31g(d,p), employed in the preceding geometry optimization step. Cu atoms were also treated with the same basis set to better capture core–valence interactions and spin density. The calculations of EPR parameters incorporated the complete mean-field SO operator for the Coulomb term. The resolution of identity (RI) [66, 67] approximation was integrated with the SO operator to enhance computational efficiency. Additionally, the calculation convergence tolerances and integration accuracies were heightened from the default settings, facilitated by the TightSCF and Grid5 options available within the software.

4.3.3. Docking Protocol. Docking calculations were executed using Gold 5.2 software, and the GoldScore function [44, 45] was employed as the scoring metric. As the protein–ligand adducts under study lacked X-ray crystallographic structures, both components were individually prepared. This process involved the use of previously DFT-optimized metallic compounds, saved as *mol2* files, and the preprocessing of PDB protein structures to facilitate interaction between the metal complex and the protein. Vacant coordination sites were virtually activated by introducing a dummy hydrogen atom positioned at a 0.75Å distance from the Cu center while preserving the coordination directionality. This approach aligns with the methodology employed in earlier studies [68, 69]. According to Lewis acid and base theory, the role of the acid acceptor transitions from the metal to the fictitious proton within the vacant site. As a result, the software interprets the metal as a hydrogen bond donor, rendering it capable of interacting with the hydrogen bond acceptors present in the protein. The genetic algorithm (GA) parameters were configured for 50 runs, with a minimum of 100,000 operations, whereas the remaining parameters were maintained at their default settings [68, 69]. We created evaluation spheres with radii of 8 and 12Å to identify potential binding sites. These spheres were centered on specific areas of interest, which comprised solvent-exposed amino acids, selected as they are the most likely to participate in coordination interactions with Cu. We used the "relSESA" calculation method, originally proposed by the Murgita group [47], to identify these binding sites. This calculation involves determining the solvent-accessible surface (SAS) value using UCSF Chimera [46]. The SAS value is then divided by individual area values imported as attributes and derived from the standard Gly–X–Gly areas calculated by the same research group. The outcome of this calculation provides a normalized "buriedness" value for each residue, indicating its degree of burial within the entire protein structure. These calculations were preliminarily performed in Myo and albumin systems, focusing on His, Glu, Gln, Asp, Asn, and Cys residue accessibility. In the case of albumin, inner cavity pockets were also considered as binding regions of interest, for which a crystallographic structure containing HSA complexed with ODA was taken as a reference (code: 1E7I [48]), removing

the buried fatty acids and exploring the empty moieties. The protein side-chain flexibility was considered during the calculations using the Gold rotamer libraries [70], while the backbone was kept fixed. Finally, the analysis of the results was facilitated using GaudiView, a user-friendly, in-house interface readily accessible from the InsiliChem webpage [71, 72]. The evaluation of the best solutions was based on two primary criteria: (i) the mean (F_{mean}) and the highest value (F_{max}) of the scoring, measured by the fitness of GoldScore (equation (2)) associated with each pose; (ii) the consideration of the percent population of the cluster including the best pose. These criteria were fundamental in identifying and selecting the most promising binding poses among the generated docking results.

$$\text{Fitness } (F) = \alpha \cdot S^{\text{ext}}_{\text{hbond}} + \beta \cdot S^{\text{ext}}_{\text{vdW}} + \gamma \cdot S^{\text{int}}_{\text{dvW}} + \delta \cdot \left(S^{\text{int}}_{\text{dvW}} - S_{\text{tors}}\right). \quad (1)$$

$$\text{Fitness } (F) = \alpha \cdot S^{\text{ext}}_{\text{hbond}} + \beta \cdot S^{\text{ext}}_{\text{vdW}} + \gamma \cdot S^{\text{int}}_{\text{hbond}} + \delta \cdot \left(S^{\text{int}}_{\text{vdW}} - S_{\text{tors}}\right). \quad (2)$$

The fitness value associated with the GoldScore scoring function had previously undergone validation in other publications [54], affirming its reliability. Within GoldScore, two integral scoring terms to consider are $S^{\text{ext}}_{\text{hbond}}$ and $S^{\text{ext}}_{\text{vdW}}$, which pertain to the evaluation of hydrogen (hbond) and vdW intermolecular interactions, respectively. $S^{\text{int}}_{\text{hbond}}$ is indicative of intramolecular hydrogen bond interactions, whereas S_{tors} plays a pivotal role in assessing the change in stability resulting from molecular torsions. The coefficients α, β, γ, and δ represent empirical constants that have been meticulously optimized to assign appropriate weights to these diverse interactions, ensuring a balanced and precise evaluation.

Data Availability Statement

The data supporting this article have been included as part of the Supporting Information.

Conflicts of Interest

The authors declare no conflicts of interest.

Author Contributions

Quim Peña and Iker Zapirain-Gysling contributed equally to this study.

Funding

This work was supported by the Ministerio de Ciencia e Innovación (Grant Numbers BIO2015-67358-C2-2-P, CTQ2015-70371-REDT, RTI2018-098027-B-C22, PID2021-127983OB-C22 PID2020 116861GB-I00 and PID2023 149492NB-I00) and also with an FPI grant for IZG (Grant Number CTQ2017-87889-P). QP acknowledges the Ministerio de Educación, Cultura y Deporte, for financial support of an FPU grant (Grant Number FPU014/07160). The authors from the UAB are members of the "Grups de Recerca de la Generalitat de Catalunya" from Direcció General de Recerca, Generalitat de Catalunya (Grant Numbers 2017SGR-864 and 2017SGR-1584 and 2021SGR00019).

Acknowledgments

This work was supported by the Ministerio de Ciencia e Innovación (Grant Numbers BIO2015-67358-C2-2-P, CTQ2015-70371-REDT, RTI2018-098027-B-C22, and PID2021-127983OB-C22) and also with an FPI grant for IZG (Grant Number CTQ2017-87889-P). QP acknowledges the Ministerio de Educación, Cultura y Deporte, for the financial support of an FPU grant (Grant Number FPU014/07160). The authors from the UAB are members of the "Grups de Recerca de la Generalitat de Catalunya" from Direcció General de Recerca, Generalitat de Catalunya (Grant Numbers 2017SGR-864 and 2017SGR-1584). Also, the Servei d'Anàlisi Química (Universitat Autònoma de Barcelona) and Spectropole facilities (Aix Marseille Université) are kindly acknowledged for allocating instrument time.

Supporting Information

Additional supporting information can be found online in the Supporting Information section. *(Supporting Information)*

Figure S1: Deconvoluted ESI-MS spectra of native proteins: HSA, Tf, Cyt, and Myo. Table S1: Experimental molecular weight (MW) of the proteins determined by ESI-MS. Table S2: Myo docking results with Cu(II) complex **C1**. Table S3: Solvent exposure of amino acids in Myo, computed by relative solvent-excluded surface area (relSESA). Table S4: Solvent exposure of amino acids in HSA, computed by relative solvent-excluded surface area (relSESA). Figure S2: Representation of the HSA inner binding cavities. Figure S3: Comparison of two different albumin docking approaches illustrated. Table S5: HSA docking results with complex **C1**. Figure S4: Square-pyramidal geometry models. Table S6: Computational EPR parameters of square-pyramidal geometry models. Figure S5: Benchmark comparison of geometries obtained from B3LYP and WB97XD functionals. Table S7: Computational EPR parameters of geometries derived from B3LYP and WB97XD functionals.

References

[1] E. J. Anthony, E. M. Bolitho, H. E. Bridgewater, et al., "Metallodrugs Are Unique: Opportunities and Challenges of Discovery and Development," *Chemical Science* 11, no. 48 (2020): 12888–12917, https://doi.org/10.1039/d0sc04082g.

[2] K. D. Mjos and C. Orvig, "Metallodrugs in Medicinal Inorganic Chemistry," *Chemistry Review* 114, no. 8 (2014): 4540–4563, https://doi.org/10.1021/cr400460s.

[3] V. Nanjappa, J. K. Thomas, A. Marimuthu, et al., "Plasma Proteome Database as a Resource for Proteomics Research: 2014 Update," *Nucleic Acids Research* 42, no. D1 (2014): D959–D965, https://doi.org/10.1093/nar/gkt1251.

[4] M. Groessl, M. Terenghi, A. Casini, L. Elviri, R. Lobinski, and P. J. Dyson, "Reactivity of Anticancer Metallodrugs with Serum Proteins: New Insights from Size Exclusion Chromatography-ICP-MS and ESI-MS," *Journal of Analytical*

Atomic Spectrometry 25, no. 3 (2010): 305–313, https://doi.org/10.1039/B922701F.

[5] A. R. Timerbaev, C. G. Hartinger, S. S. Aleksenko, and B. K. Keppler, "Interactions of Antitumor Metallodrugs with Serum Proteins: Advances in Characterization Using Modern Analytical Methodology," *Chemistry Review* 106, no. 6 (2006): 2224–2248, https://doi.org/10.1021/cr040704h.

[6] D. Loreto, G. Ferraro, and A. Merlino, "Protein-metallodrugs Interactions: Effects on the Overall Protein Structure and Characterization of Au, Ru and Pt Binding Sites," *International Journal of Biological Macromolecules* 163 (2020): 970–976, https://doi.org/10.1016/j.ijbiomac.2020.07.053.

[7] A. I. Ivanov, J. Christodoulou, J. A. Parkinson, et al., "Cisplatin Binding Sites on Human Albumin," *Journal of Biological Chemistry* 273, no. 24 (1998): 14721–14730, https://doi.org/10.1074/jbc.273.24.14721.

[8] G. Ferraro and A. Merlino, "Metallodrugs: Mechanisms of Action, Molecular Targets and Biological Activity," *International Journal of Molecular Sciences* 23, no. 7 (2022): 3504–3509, https://doi.org/10.3390/ijms23073504.

[9] T. Bohnert and L. S. Gan, "Plasma Protein Binding: from Discovery to Development," *Journal of Pharmaceutical Sciences* 102, no. 9 (2013): 2953–2994, https://doi.org/10.1002/jps.23614.

[10] A. Merlino, "Metallodrug Binding to Serum Albumin: Lessons from Biophysical and Structural Studies," *Coordination Chemistry Reviews* 480 (2023): 215026, https://doi.org/10.1016/j.ccr.2023.215026.

[11] M. Paul, A. M. Itoo, B. Ghosh, and S. Biswas, "Current Trends in the Use of Human Serum Albumin for Drug Delivery in Cancer," *Expert Opinion on Drug Delivery* 19, no. 11 (2022): 1449–1470, https://doi.org/10.1080/17425247.2022.2134341.

[12] Y.-R. Zheng, K. Suntharalingam, T. C. Johnstone, et al., "Pt(IV) Prodrugs Designed to Bind Non-Covalently to Human Serum Albumin for Drug Delivery," *Journal of the American Chemical Society* 136, no. 24 (2014): 8790–8798, https://doi.org/10.1021/ja5038269.

[13] D. B. Kitchen, H. Decornez, J. R. Furr, and J. Bajorath, "Docking and Scoring in Virtual Screening for Drug Discovery: Methods and Applications," *Nature Reviews Drug Discovery* 3 (2004): 935–949, https://doi.org/10.1038/nrd1549.

[14] A. R. Leach, B. K. Shoichet, and C. E. Peishoff, "Prediction of Protein-Ligand Interactions. Docking and Scoring: Successes and Gaps," *Journal of Medicinal Chemistry* 49, no. 20 (2006): 5851–5855, https://doi.org/10.1021/jm060999m.

[15] M. Diéguez, J.-E. Bäckvall, O. Pàmies, et al., "Computational Studies of Artificial Metalloenzymes: From Methods and Models to Design and Optimization," *Artificial Metalloenzymes and metalloDNAnzymes in Catalysis*, eds. M. Diéguez, J.-E. Bäckvall, and O. Pàmies (2018), https://doi.org/10.1002/9783527804085.ch4.

[16] J. C. Pessoa, E. Garribba, M. F. A. Santos, and T. Santos-Silva, "Vanadium and Proteins: Uptake, Transport, Structure, Activity and Function," *Coordination Chemistry Reviews* 301 (2015): 49–86, https://doi.org/10.1016/j.ccr.2015.03.016.

[17] S. Vázquez-Rodríguez, D. Ramírez-Contreras, L. Noriega, et al., "Interaction of Copper Potential Metallodrugs With TMPRSS2: A Comparative Study of Docking Tools and Its Implications on COVID-19," *Frontiers of Chemistry* 11 (2023): 1128859, https://doi.org/10.3389/fchem.2023.1128859.

[18] S. Tabassum, W. M. Al-Asbahy, M. Afzal, and F. Arjmand, "Synthesis, Characterization and Interaction Studies of Copper-Based Drug with Human Serum Albumin (HSA): Spectroscopic and Molecular Docking Investigations," *Journal of Photochemistry and Photobiology B: Biology* 114 (2012): 132–139, https://doi.org/10.1016/j.jphotobiol.2012.05.021.

[19] Q. Peña, S. Rodríguez-Calado, A. J. Simaan, et al., "Cell-Penetrating Peptide-Conjugated Copper Complexes for Redox-Mediated Anticancer Therapy," *Frontiers in Pharmacology* 13 (2022): 1060827, https://doi.org/10.3389/fphar.2022.1060827.

[20] Q. Peña, G. Sciortino, J.-D. Maréchal, et al., "Copper(II) N,N,O-chelating Complexes as Potential Anticancer Agents," *Inorganic Chemistry* 60, no. 5 (2021): 2939–2952, https://doi.org/10.1021/acs.inorgchem.0c02932.

[21] Q. Peña, "Novel Cu(II) Complexes Bearing N,O-Donor Heteroaromatic Ligands as Potential Anticancer Drugs: A Redox-Active Metallic Core," (Universitat Autònoma de Barcelona, 2020), PhD Thesis.

[22] S. Weiskirchen, S. K. Schröder, E. M. Buhl, and R. Weiskirchen, "A Beginner's Guide to Cell Culture: Practical Advice for Preventing Needless Problems," *Cells* 12 (2023): 682, https://doi.org/10.3390/cells12050682.

[23] S. K. Hoffmann, J. Goslar, S. Lijewski, and A. Zalewska, "EPR and ESE of CuS4 Complex in Cu(dmit)2: G-Factor and Hyperfine Splitting Correlation in Tetrahedral Cu-Sulfur Complexes," *Journal of Magnetic Resonance* 236 (2013): 7–14, https://doi.org/10.1016/j.jmr.2013.08.009.

[24] J. Peisach and W. E. Blumberg, "Structural Implications Derived From the Analysis of Electron Paramagnetic Resonance Spectra of Natural and Artificial Copper Proteins," *Archives of Biochemistry and Biophysics* 165, no. 2 (1974): 691–708, https://doi.org/10.1016/0003-9861(74)90298-7.

[25] U. Sakaguchi and A. W. Addison, "Spectroscopic and Redox Studies of Some Copper(II) Complexes With Biomimetic Donor Atoms: Implications for Protein Copper Centres," *Journal of the Chemical Society Dalton Transactions* no. 4 (1979): 600–608, https://doi.org/10.1039/DT9790000600.

[26] A. M. N. Silva, T. Moniz, B. de Castro, and M. Rangel, "Human Transferrin: An Inorganic Biochemistry Perspective," *Coordination Chemistry Reviews* 449 (2021): 214186, https://doi.org/10.1016/j.ccr.2021.214186.

[27] R. N. Moman, N. Gupta, and M. Varacallo, "Physiology, Albumin," https://www.ncbi.nlm.nih.gov/books/NBK459198/.

[28] M. T. Wilson, Reeder, and B. J. Myoglobin, *Encyclopedia of Respiratory Medicine* (Elsevier, 2006).

[29] G. A. Ordway and D. J. Garry, "Myoglobin: An Essential Hemoprotein in Striated Muscle," *Journal of Experimental Biology* 207, no. 20 (2004): 3441–3446, https://doi.org/10.1242/jeb.01172.

[30] X. Jiang and X. Wang, "Cytochrome **C**-Mediated Apoptosis," *Annual Review of Biochemistry* 73, no. 1 (2004): 87–106, https://doi.org/10.1146/annurev.biochem.73.011303.073706.

[31] K. G. Samper, V. Rodríguez, E. Ortega-Carrasco, et al., "Understanding the Interaction of an Antitumoral Platinum(II) 7-azaindolate Complex With Proteins and DNA," *Biometals* 27, no. 6 (2014): 1159–1177, https://doi.org/10.1007/s10534-014-9780-1.

[32] K. G. Samper, C. Vicente, V. Rodríguez, et al., "Studying the Interactions of a Platinum(II) 9-Aminoacridine Complex With Proteins and Oligonucleotides by ESI-TOF MS," *Dalton Transactions* 41, no. 1 (2012): 300–306, https://doi.org/10.1039/C1DT11506E.

[33] M. E. Del Castillo Busto, J. Meija, M. Montes-Bayón, and A. Sanz-Medel, "Diophantine Analysis Complements Electrospray-Q-TOF Data for Structure Elucidation of Transferrin Glycoforms Used for Clinical Diagnosis in Human Serum and

Cerebrospinal Fluid," *Proteomics* 9, no. 4 (2009): 1109–1113, https://doi.org/10.1002/pmic.200701182.

[34] W. Bal, M. Sokołowska, E. Kurowska, and P. Faller, "Binding of Transition Metal Ions to Albumin: Sites, Affinities and Rates," *Biochimica et Biophysica Acta (BBA): General Subjects* 1830, no. 12 (2013): 5444–5455, https://doi.org/10.1016/j.bbagen.2013.06.018.

[35] C. Harford and B. Sarkar, "Amino Terminal Cu(II)- and Ni(II)-Binding (ATCUN) Motif of Proteins and Peptides: Metal Binding, DNA Cleavage, and Other Properties," *Accounts of Chemical Research* 30, no. 3 (1997): 123–130, https://doi.org/10.1021/ar9501535.

[36] M.-E. Llases, M. N. Morgada, and A. J. Vila, "Biochemistry of Copper Site Assembly in Heme-Copper Oxidases: A Theme With Variations," *International Journal of Molecular Sciences* 20, no. 15 (2019): 3830–3848, https://doi.org/10.3390/ijms20153830.

[37] J. E. Wertz and J. R. Bolton, *Electron Spin Resonance: Elementary Theory and Practical Applications* (NewYork: Chapman & Hall, 1986).

[38] G. Sciortino, J.-D. Maréchal, I. Fábián, N. Lihi, and E. Garribba, "Quantitative Prediction of Electronic Absorption Spectra of Copper (II)–Bioligand Systems: Validation and Applications," *Journal of Inorganic Biochemistry* 204 (2020): 110953, https://doi.org/10.1016/j.jinorgbio.2019.110953.

[39] E. Garribba and G. Micera, "The Determination of the Geometry of Cu(II) Complexes: An EPR Spectroscopy Experiment," *Journal of Chemical Education* 83, no. 8 (2006): 1229–1282, https://doi.org/10.1021/ed083p1229.

[40] J. Gaăzo, I. B. Bersuker, J. Garaj, et al., "Plasticity of the Coordination Sphere of Copper(II) Complexes, its Manifestation and Causes," *Coordination Chemistry Reviews* 19 (1976): 253–297, https://doi.org/10.1016/S0010-8545(00)80317-3.

[41] F. A. Taiwo, "Electron Paramagnetic Resonance Spectroscopic Studies of Iron and Copper Proteins," *Journal of Spectroscopy* 17, no. 1 (2003): 53–63, https://doi.org/10.1155/2003/673567.

[42] G. Sciortino, G. Lubinu, J. D. Maréchal, and E. Garribba, "DFT Protocol for EPR Prediction of Paramagnetic Cu (II) Complexes and Application to Protein Binding Sites," *Magnetochemistry* 4 (2018): 55, https://doi.org/10.3390/magnetochemistry4040055.

[43] G. Sciortino, E. Garribba, J. Rodriguez-Guerra Pedregal, and J. D. Marechal, "Simple Coordination Geometry Descriptors Allow to Accurately Predict Metal-Binding Sites in Proteins," *ACS Omega* 4, no. 2 (2019): 3726–3731, https://doi.org/10.1021/acsomega.8b03457.

[44] G. Jones, P. Willett, R. C. Glen, A. R. Leach, and R. Taylor, "Development and Validation of a Genetic Algorithm for Flexible Docking 1 1Edited by F. E. Cohen," *Journal of Molecular Biology* 267, no. 3 (1997): 727–748, https://doi.org/10.1006/jmbi.1996.0897.

[45] G. Jones, P. Willett, and R. C. Glen, "Molecular Recognition of Receptor Sites Using a Genetic Algorithm with a Description of Desolvation," *Journal of Molecular Biology* 245, no. 1 (1995): 43–53, https://doi.org/10.1016/s0022-2836(95)80037-9.

[46] E. F. Pettersen, T. D. Goddard, C. C. Huang, et al., "UCSF Chimera—A Visualization System for Exploratory Research and Analysis," *Journal of Computational Chemistry* 25, no. 13 (2004): 1605–1612, https://doi.org/10.1002/jcc.20084.

[47] C. J. Bendell, S. Liu, T. Aumentado-Armstrong, et al., "Transient Protein-Protein Interface Prediction: Datasets, Features, Algorithms, and the RAD-T Predictor," *BMC Bioinformatics* 15 (2014): 82–12, https://doi.org/10.1186/1471-2105-15-82.

[48] A. A. Bhattacharya, T. Grüne, and S. Curry, "Crystallographic Analysis Reveals Common Modes of Binding of Medium and Long-Chain Fatty Acids to Human Serum Albumin 1 1Edited by R. Huber," *Journal of Molecular Biology* 303, no. 5 (2000): 721–732, https://doi.org/10.1006/jmbi.2000.4158.

[49] G. Sciortino, D. Sanna, V. Ugone, J. D. Maréchal, and E. Garribba, "Integrated ESI-MS/EPR/Computational Characterization of the Binding of Metal Species to Proteins: Vanadium Drug–Myoglobin Application," *Inorganic Chemistry Frontiers* 6 (2019): 1561–1578, https://doi.org/10.1039/c9qi00179d.

[50] G. Sciortino, D. Sanna, V. Ugone, et al., "Elucidation of Binding Site and Chiral Specificity of Oxidovanadium Drugs With Lysozyme through Theoretical Calculations," *Inorganic Chemistry* 56, no. 21 (2017): 12938–12951, https://doi.org/10.1021/acs.inorgchem.7b01732.

[51] W. Li, H. Xie, Y. Huang, L. Song, Y. Shao, and K. Qiu, "Application of Gaussian 09/GaussView 5.0 in Analytical Chemistry Teaching," *J. Kunming Med. Univ*. (2016): 134–136.

[52] Gaussian, C. Revision, M. J. Frisch, et al., in *Gaussian, Inc* (2016).

[53] A. D. Becke, "Density-Functional Thermochemistry. III. The Role of Exact Exchange," *The Journal of Chemical Physics* 98, no. 7 (1993): 5648–5652, https://doi.org/10.1063/1.464913.

[54] C. Lee, W. Yang, and R. G. Parr, "Development of the Colle-Salvetti Correlation-Energy Formula into a Functional of the Electron Density," *Physical Review B: Condensed Matter* 37, no. 2 (1988): 785–789, https://doi.org/10.1103/physrevb.37.785.

[55] S. Grimme, J. Antony, S. Ehrlich, and H. Krieg, "A Consistent and Accurate Ab Initio Parametrization of Density Functional Dispersion Correction (DFT-D) for the 94 Elements H-Pu," *The Journal of Chemical Physics* 132, no. 15 (2010): 154104, https://doi.org/10.1063/1.3382344.

[56] V. A. Rassolov, M. A. Ratner, J. A. Pople, P. C. Redfern, and L. A. Curtiss, "6-31G Basis Set for Third-row Atoms," *Journal of Computational Chemistry* 22, no. 9 (2001): 976–984, https://doi.org/10.1002/jcc.1058.

[57] S. F. Sousa, G. R. Pinto, A. J. Ribeiro, J. T. Coimbra, P. A. Fernandes, and M. J. Ramos, "Comparative Analysis of the Performance of Commonly Available Density Functionals in the Determination of Geometrical Parameters for Copper Complexes," *Journal of Computational Chemistry* 34, no. 24 (2013): 2079–2090, https://doi.org/10.1002/jcc.23349.

[58] M. Buhl, C. Reimann, D. A. Pantazis, T. Bredow, and F. Neese, "Geometries of Third-Row Transition-Metal Complexes From Density-Functional Theory," *Journal of Chemical Theory and Computation* 4, no. 9 (2008): 1449–1459, https://doi.org/10.1021/ct800172j.

[59] M. Bühl and H. Kabrede, "Geometries of Transition-Metal Complexes from Density-Functional Theory," *Journal of Chemical Theory and Computation* 2, no. 5 (2006): 1282–1290, https://doi.org/10.1021/ct6001187.

[60] D. J. Kissick, C. M. Dettmar, M. Becker, et al., "Towards Protein-Crystal Centering Using Second-Harmonic Generation (SHG) Microscopy," *Acta Crystallographica Section D Biological Crystallography* 69, no. 5 (2013): 843–851, https://doi.org/10.1107/S0907444913002746.

[61] S. Sugio, A. Kashima, S. Mochizuki, M. Noda, and K. Kobayashi, "Crystal Structure of Human Serum Albumin at 2.5 Å Resolution," *Protein Engineering Design and Selection* 12, no. 6 (1999): 439–446, https://doi.org/10.1093/protein/12.6.439.

[62] D. C. Bas, D. M. Rogers, and J. H. Jensen, "Very Fast Prediction and Rationalization of pKa Values for Protein–Ligand

Complexes," *Proteins: Structure, Function, and Bioinformatics* 73, no. 3 (2008): 765–783, https://doi.org/10.1002/prot.22102.

[63] F. Neese, "Software Update: The ORCA Program System—Version 5.0," *WIREs Computational Molecular Science* 12, no. 5 (2022): e1606, https://doi.org/10.1002/wcms.1606.

[64] F. Neese, "The ORCA Program System," *WIREs Computational Molecular Science* 2, no. 1 (2012): 73–78, https://doi.org/10.1002/wcms.81.

[65] C. Adamo and V. Barone, "Toward Reliable Density Functional Methods without Adjustable Parameters: The PBE0 Model," *The Journal of Chemical Physics* 110, no. 13 (1999): 6158–6170, https://doi.org/10.1063/1.478522.

[66] F. Neese, "An Improvement of the Resolution of the Identity Approximation for the Formation of the Coulomb Matrix," *Journal of Computational Chemistry* 24, no. 14 (2003): 1740–1747, https://doi.org/10.1002/jcc.10318.

[67] R. A. Kendall and H. A. Früchtl, "The Impact of the Resolution of the Identity Approximate Integral Method on Modern Ab Initio Algorithm Development," *Theoretical Chemistry Accounts: Theory, Computation, and Modeling* 97, no. 1-4 (1997): 158–163, https://doi.org/10.1007/s002140050249.

[68] G. Sciortino, J. Rodríguez-Guerra Pedregal, A. Lledós, E. Garribba, and J. D. Maréchal, "Prediction of the Interaction of Metallic Moieties with Proteins: An Update for Protein-ligand Docking Techniques," *Journal of Computational Chemistry* 39, no. 1 (2018): 42–51, https://doi.org/10.1002/jcc.25080.

[69] G. Sciortino, E. Garribba, and J. D. Maréchal, "Validation and Applications of Protein–Ligand Docking Approaches Improved for Metalloligands with Multiple Vacant Sites," *Inorganic Chemistry* 58, no. 1 (2018): 294–306, https://doi.org/10.1021/acs.inorgchem.8b02374.

[70] S. C. Lovell, J. M. Word, J. S. Richardson, and D. C. Richardson, "The Penultimate Rotamer Library," *Proteins: Structure, Function, and Genetics* 40, no. 3 (2000): 389–408.

[71] J. Rodríguez-Guerra Pedregal, *Insilichem/Gaudiview: Pre-Alpha Public Release* (Zenodo, 2017).

[72] J. Rodríguez-Guerra Pedregal, G. Sciortino, J. Guasp, M. Municoy, and J. D. Maréchal, "GaudiMM: A Modular Multi-objective Platform for Molecular Modeling," *Computational Chemistry* 38 (2017): 2118–2126, https://doi.org/10.1002/jcc.24847.